

Gait Modification and Optimization using Neural Network-Genetic Algorithm Approach: Application to Knee Rehabilitation

Marzieh.M.Ardestani^{1,*}, Mehran Moazen² and Zhongmin Jin^{1,3}

¹ *State Key Laboratory for Manufacturing System Engineering, School of Mechanical Engineering, Xi'an Jiao tong University, 710054, Xi'an, Shaanxi, China*

² *Medical and Biological Engineering, School of Engineering, University of Hull, Hull, UK*

³ *Institute of Medical and Biological Engineering, School of Mechanical Engineering, University of Leeds, Leeds, LS2 9JT, UK*

*Corresponding author Tel.: +0-86-029-83395122;

E-mail: mostafavizadeh@yahoo.com

Abstract

Gait modification strategies play an important role in the overall success of total knee arthroplasty. There are a number of studies based on multi-body dynamic (MBD) analysis that have minimized knee adduction moment to offload knee joint. Reducing the knee adduction moment, without consideration of the actual contact pressure, has its own limitations. Moreover, MBD-based framework that mainly relies on iterative trial-and-error analysis, is fairly time consuming. This study embedded a time-delay neural network (TDNN) in a genetic algorithm (GA) as a cost effective computational framework to minimize contact pressure. Multi-body dynamics and finite element analyses were performed to calculate gait kinematics/kinetics and the resultant contact pressure for a number of experimental gait trials. A TDNN was trained to learn the nonlinear relation between gait parameters (inputs) and contact pressures (output). The trained network was then served as a real-time cost function in a GA-based global optimization to calculate contact pressure associated with each potential gait pattern. Two optimization problems were solved: first, knee flexion angle was bounded within the normal patterns and second, knee flexion angle was allowed to be increased beyond the normal walking. Designed gait patterns were evaluated through multi-body dynamics and finite element analyses.

The TDNN-GA resulted in realistic gait patterns, compared to literature, which could effectively reduce contact pressure at the medial tibiofemoral knee joint. The first optimized gait pattern reduced the knee contact pressure by up to 21% through modifying the adjacent joint kinematics whilst knee flexion was preserved within normal walking. The second optimized gait pattern achieved a more effective pressure reduction (25%) through a slight increase in the knee flexion at the cost of considerable increase in the ankle joint forces. The proposed approach is a cost-effective computational technique that can be used to design a variety of rehabilitation strategies for different joint replacement with multiple objectives.

Keywords: Gait modification, Tibiofemoral knee joint, Time delay neural network, Genetic algorithm, Contact pressure

1 **1. Introduction:**

2 Following total knee arthroplasty (TKA), rehabilitation strategies are of significant importance to accelerate
3 patient recovery(Isaac et al., 2005, Klein et al., 2008), reinforce joint functionality(Moffet et al., 2004, Rahmann et al.,
4 2009), decrease gait asymmetry(Zeni Jr et al., 2011), and augment the durability and life time of knee
5 prostheses(Fransen, 2011, Mont et al., 2006). Gait rehabilitations mainly aim to decrease knee joint loading through
6 minor changes in human gait patterns. However, recognizing the synergistic kinematic changes, required for joint
7 offloading, is a challenging task, hence; computational approaches have been used to facilitate the design procedure.
8 To best of our knowledge, most of the current literature on gait modification strategies have been designed through
9 multi-body dynamic (MBD) analysis (Barrios et al., 2010, Barrios and Davis, 2007, Fregly et al., 2009, Hunt et al.,
10 2008, Mündermann et al., 2008, Willson et al., 2001, Ackermann and van den Bogert, 2010, Anderson and Pandy, 2001,
11 Fregly et al., 2007) . However, iterative “trial-and-error” MBD analysis, that has been performed in such studies,, is
12 fairly time demanding which limits the applicability and generality of the method. Hence, a cost-effective
13 computational framework that minimizes the computational cost is of particular interest.

14 Besides the computational cost, there are a number of aspects that have not been well addressed by the
15 conventional MBD-based framework. *First* , MBD-based approach attempts to reduce the peak values of knee
16 adduction moment (KAM) which is not always a reliable measure since decreasing KAM may not necessarily decrease
17 knee joint loading (Walter et al., 2010); and the results of such approach are sensitive to the chosen reference frame
18 (e.g. laboratory, floating reference frames) (Lin et al., 2001, Shull et al., 2012). *Second* , joint-offloading gait patterns
19 are likely to decrease the contact area of articulating surfaces that unfavorably may increase the contact pressure at the
20 knee joint (D'Lima et al., 2008). Therefore, reducing the contact pressure should be concerned as the principal goal of
21 rehabilitation design. Conventional computational frameworks however are inherently unable consider the contact
22 pressure in the design procedure since the conventional methods require an explicit cost function whilst the relation
23 between gait kinematics and the resultant contact pressure has not been stated explicitly before. Also considering the
24 contact pressure necessitates using the intensive finite element analysis (FEA) which in turn increases the
25 computational cost (Halloran et al., 2010). A cost-effective surrogate which releases the necessity of iterative FEA is
26 therefore of significant advantage. *Third*, previous studies could not reach a general consensus about the contribution
27 of knee flexion to the knee joint offloading. Knee flexion is a key synergetic parameter that is often increased within
28 the clinical execution of the rehabilitation patterns (Barrios et al., 2010, Fregly et al., 2007, van den Noort et al., 2013).
29 Several studies concluded that increasing the knee flexion would reduce KAM (Fregly et al., 2009), whilst others

30 showed that it has no association with KAM (Creaby et al., 2013) or may even increase contact pressure at the knee
31 bearing surfaces (D'Lima et al., 2008). A systematic investigation is required to enhance our understanding of the
32 contribution of knee flexion to the knee joint offloading.

33 Artificial neural networks (ANN) and genetic algorithm (GA) are two relatively new techniques in the field of
34 biomechanics. Artificial neural network (ANN) can be used as a real-time surrogate model with the ability to *learn* a
35 nonlinear relationship. Once a set of inputs and corresponding outputs are presented to the network, the network learns
36 the causal interactions between inputs and outputs. Given a new set of inputs, the trained neural network (surrogate
37 model) can generalize the relationship to produce the associated outputs. The ANN surrogate therefore can be of
38 significant advantage especially when the original model necessitates repeating a time-consuming computation. For
39 example, ANN has been widely used as a surrogate of FEA (Campoli et al., 2012, Hambli, 2010, Hambli, 2011, Naito
40 and Torii, 2005, Lu et al., 2013, Simic et al., 2011, Zadpoor et al., 2012). Genetic algorithm is a time-efficient global
41 optimization technique which searches the entire data space to find the best solution (Goldberg, 1989). In each iteration,
42 only potential candidates that better optimize the cost function will survive to the next iteration. Thus, regardless of the
43 initial point, the search data space is iteratively modified and GA will rapidly converge to the global optimum solution.
44 This in turn assures the robustness of the method and minimizes the computational effort required to find the best
45 solution. Moreover, GA is capable of dealing with multivariable data space, nonlinear input-output interactions and
46 non-explicit, non-differential cost function.

47 Therefore, the overall aim of this study was to develop a hybrid framework of time delay neural network
48 (TDNN) and genetic algorithm (GA) to address the aforementioned limitations of the literature. In particular this study
49 aimed to (1) optimize the gait pattern in order to minimize the contact pressure at the knee articulating surfaces and (2)
50 investigate the role of knee flexion in knee joint offloading. The advantage of the proposed approach was also compared
51 over the existing knee rehabilitations in the literature.

52 **2. Materials and methods**

53 The proposed computational approach was implemented in the following steps:

54 *Step 1)* Experimental gait analysis data were obtained from the literature (Section 2.1), and imported into MBD analysis
55 to calculate gait kinematics and kinetics (Section 2.2). Knee flexion angle and three dimensional knee joint loadings,
56 taken from MBD, in turn served as boundary condition and loading profiles of a finite element simulation to calculate
57 contact pressure (Section 2.3). Gait trials were then outlined via a number of kinematic features and the corresponding
58 maximum contact pressure values (CPRESS-max) (Section 2.4).

59 *Step 2)* A time-delay neural network (TDNN) was trained to learn the nonlinear relationship between kinematic features
60 as inputs and the corresponding CPRESS-max values as output (Section 2.5).

61 *Step 3)* A genetic algorithm (GA) was implemented to search for the optimum kinematic features (optimization
62 variables) which minimized the CPRESS-max at the knee joint bearing surfaces. In this GA, the trained TDNN was
63 served as a real-time cost function to calculate the objective value (CPRESS-max) (Section 2.6).

64 **2.1. Experimental gait data**

65 Experimental gait analysis data of a single subject with unilateral TKA (female, height 167 cm, mass 78.4 kg)
66 was obtained from the literature (<https://simtk.org/home/kneeloads>; accessed on June 2013). The subject walked with
67 a variety of different gait patterns including *normal*, *medial thrust*, *trunk sway*, *walking pole*, *bouncy*, *crouch*, *smooth*
68 and *fore foot strike*. *Medial thrust*, *trunk sway* and *walking pole* were knee rehabilitation strategies, designed to
69 decrease KAM, whilst the remaining gait trials were exaggerated walking patterns to cover the span of executable gait
70 for the subject. Compared to *normal* walking, the subject walked with a slightly decreased pelvis obliquity, slightly
71 increased pelvis axial rotation and leg flexion to implement *medial thrust* pattern. For *trunk sway* pattern, the subject
72 walked with an increased lateral leaning of the trunk in the frontal plane over the standing leg. In *walking pole*, the
73 subject used bilateral poles as walking aids. For each gait pattern, five gait trials were repeated under the same walking
74 condition at a self-selected pace. A total of two complete gait cycles were picked up from each trial, leading to a total
75 of 84 data sets. For further details, see (Fregly et al., 2012). Gait trials were recorded in terms of marker trajectory data
76 (Motion Analysis Corp., Santa Rosa, CA) and ground reaction forces (AMTI Corp., Watertown, MA).

77 **2.2. Multi-body dynamics**

78 Experimental ground reaction forces and marker trajectories were imported into the three-dimensional multi-
79 body dynamics simulation software, AnyBody Modelling System (version 5.2, AnyBody Technology, Aalborg,
80 Denmark). A lower extremity musculoskeletal model was used in AnyBody software based on the University of Twente
81 Lower Extremity Model (TLEM) (Klein Horsman, 2007). This model, available in the AnyBody published repository,
82 had 160 muscle units as well as foot, thigh, patella, shank, trunk and thorax segments. Hip joint was modelled as a
83 spherical joint with three degrees of freedom (DOF): flexion-extension, abduction-adduction and internal-external
84 rotation. Knee joint was modelled as a hinge joint with only one DOF for flexion-extension and universal joint was
85 considered for ankle-subtalar complex. Since the assumptions of the simplified knee joint and rigid multi-bodies were
86 made, the detailed knee implant was not considered in the MBD analysis. Knee flexion angle and three dimensional
87 knee joint loads, aligned in medial-lateral, proximal-distal and anterior-posterior directions, were calculated for each

88 complete gait cycle. A complete gait cycle was defined as the time period from heel strike of one leg to the following
89 heel strike of the same leg (Vaughan et al., 1992). Computations were then normalized to 100 samples to represent one
90 complete gait cycle. Knee flexion and three dimensional knee joint loads then served as the boundary condition and
91 load profiles for FEA.

92 **2.3. Finite element method**

93 A typical tibiofemoral knee implant was modelled in the commercial finite element package;
94 ABAQUS/Explicit (version 6.12 Simulia Inc., Providence, RI) using the computer aided design (CAD) of a clinically
95 available fixed bearing knee implant. The knee implant consisted of two main parts; femoral component and tibia insert.
96 Rigid body assumptions were applied to both parts, with a simple linear elastic foundation model defined between the
97 two contacting bodies (Halloran et al., 2005). Tetrahedral (C3D10M) elements were used to mesh the model in
98 ABAQUS. Convergence was tested by decreasing the element size from 8 mm to 0.5 mm in five steps (8, 4, 2, 1, and
99 0.5 mm). The solution converged on contact pressure ($\leq 5\%$) with over 86000 and 44000 elements representing the
100 femoral component and the tibia insert respectively. This was also consistent with the previous mesh convergence
101 studies for similar finite element models (Abdelgaied et al., 2011, Halloran et al., 2005). The physical interaction
102 between femoral component and tibia insert was taken into account as a surface-to-surface contact (femur as the master
103 surface and tibia as the slave surface) through a penalty-based approach with an isotropic friction coefficient of 0.04
104 (Abdelgaied et al., 2011, Halloran et al., 2005). The tibia insert was constrained in all available DOFs and the femoral
105 component was only allowed for flexion-extension under the three dimensional load which were obtained from MBD
106 analysis. The model calculated the contact pressure at each node for each time increment. An output field was created
107 over all simulation frames to compute the maximum value of the contact pressures (CPRESS_max) over the entire gait
108 cycle. Since the medial compartment experiences the CPRESS-max value (Schipplein and Andriacchi, 1991), this part
109 was considered for the rest of the study (Figure 1a).

110 **2.4. Feature extraction**

111 During a complete gait cycle, the extent to which a joint can be moved (range of motion) and the corresponding
112 absolute values of motions directly affect the quality of human gait and joint loading. For example, increasing the
113 “*maximum*” value of hip adduction angle or hip internal rotation would decrease the “*peak*” values of KAM (Barrios
114 et al., 2010). On the other hand, to design a realistic gait modification strategy, the overall trend of kinematic patterns
115 cannot differ significantly from natural human walking habitudes; otherwise the pattern would not be acceptable and
116 executable by the patient. Thus, only the key features of kinematic waveforms are needed to be modified whilst the

117 overall trends should be preserved consistent. Gait kinematics were therefore outlined through a total of 39 descriptive
 118 kinematic features (Table 1 and Figure 1b). These features have been suggested in the literature for a number of studies
 119 such as gait analysis (Collins et al., 2009, Gates et al., 2012a, Gates et al., 2012b), gait classification (Armand et al.,
 120 2006) , evaluation of joint loading (Simonsen et al., 2010), and joint inter-coordination (Wang et al., 2009).
 121 Kinematic features (optimization variables) were then allowed to vary within the corresponding ranges of experimental
 122 values plus $\pm 20\%$ variations to cover a thorough span of executable movement patterns for the subject. Contact pressure
 123 was also characterized by the maximum pressure value occurred over the entire gait cycle (CPRESS-max).

124 2.5. Time-delay neural network

125 Time delay neural network (TDNN) was implemented to model the highly nonlinear relationship between
 126 kinematic features (39 inputs) and CPRESS-max values (one output). The trained network was then embedded in an
 127 optimization process (GA) as a real-time cost function to calculate the objective values (CPRESS-max). The TDNN
 128 architecture consisted of a feed forward neural network in which a tapped delay line was added to the input layer
 129 (Figure 2). Similar to other types of neural networks, a number of processor units (neurons) were arranged in a certain
 130 configuration (layers). A weighted sum of all inputs was fed into each hidden neuron where an activation function acted
 131 on this weighted sum to produce the output of the hidden neuron. All of the hidden neurons were activated using
 132 “hyperbolic tangent sigmoid” function which linearly scaled its input signal to [-1, 1] interval:

$$133 \quad y_j^m = \frac{2}{1 + \exp(-2 * V_j^m)} - 1 \quad j = 1, 2, \dots, M_m \quad (1)$$

134 Where y_j^m is the output of j^{th} hidden neuron located at the m^{th} hidden layer, M_m is the number of hidden neurons
 135 at the m^{th} hidden layer, and $V_j^m(n)$ is the weighted sum of the signals from the previous layer which was fed to the j^{th}
 136 hidden neuron of m^{th} hidden layer:

$$137 \quad V_j^m = \sum_{k=1}^{M_{m-1}} (y_k^{m-1} * W_{jk}) + b_j \quad j = 1, 2, \dots, M_m, \quad k = 1, 2, \dots, M_{m-1} \quad (2)$$

138 Where W_{jk} is the weight relating the output of k^{th} neuron located at the $(m-1)^{th}$ layer (y_k^{m-1}) to the j^{th} hidden neuron at
 139 the m^{th} hidden layer with the bias value of b_j , and M_m and M_{m-1} are the number of neurons at the m^{th} and $(m-1)^{th}$ layers
 140 respectively. A weighted sum of all hidden neurons’ outputs was also fed into the single output node which was
 141 activated by a “pure line” function:

$$y_{out} = \sum_{k=1}^{M_m} w_k y_k^m + \bar{y} \quad (3)$$

in which \bar{y} is the output bias .

TDNN was trained using the scaled conjugate gradient algorithm (SCG) (Møller, 1993). The available data space, obtained from MBD and FEA, was randomly divided into three main parts: train (70%), validation (15%) and test (15%) subsets. The train and validation subsets were used to train the network whilst the test subset was not included in training. The network prediction error on the validation subset implied how accurate the network has learned the input-output causal relationship (accuracy). On the other hand, the network prediction error on the test subset indicated the extent to which the trained network could generalize this causal relationship for the new inputs (generality). Generally speaking, the structure of the FFANN would build a trade-off between “*prediction accuracy*” and “*generality*”. Whilst increasing the number of hidden neurons/layers would increase the prediction accuracy, using too many neurons would decrease the generality and increase the test error. The number of hidden layers and hidden neurons were therefore determined according to the network prediction error for the test and validation subsets. The input delay was also determined by trial and error.

2.6. Genetic algorithm

In the present study, gait optimization was stated as follows:

$$\text{Minimize } Y : Y=U(X) \quad AX \leq b \quad , \quad X_L \leq X \leq X_U \quad (4)$$

Where Y is the CPRESS-max, X is the optimization variables (kinematic features), and U is the trained TDNN. Upper and lower bounds of the optimization variables (X_L and X_U) were obtained from the experimental gait trials plus $\pm 20\%$ variations. Matrix A and vector b described the linear inequality constraints in order to control the natural trends of the gait kinematics (Appendix). Genetic algorithm (GA) was used to search for those kinematic features that could minimize CPRESS-max. Kinematic features (optimization variables) were configured as $1*N$ arrays called individuals ($N=39$). In each iteration, the GA created a population of individuals and then employed the trained TDNN to calculate the resultant CPRESS-max values associated with potential individuals. Those individuals that led to lower CPRESS-max values were assigned a higher survivorship probability to be selected and make the next population. Each individual is indeed a potential solution and each population is a search space of solutions. Accordingly, after passing several iterations, the population (solution search space) evolved toward the optimized individuals.

168 The first population was initialized with random individuals in which features of gait kinematics were
169 randomly chosen due to X_L and X_U . The next populations were created through selected individuals by elitism, crossover
170 and mutation operators of GA (Goldberg, 1989). Table 2 summarizes the setting of the proposed GA in MATLAB
171 (v.2009, Genetic Algorithm toolbox). In the present study, two systematic optimizations were performed: *first*, knee
172 flexion was bounded to vary within the *normal* walking. *Second*, the knee flexion was allowed to vary beyond the
173 *normal* walking up to the *medial thrust* pattern. Once the GA converged to the optimum kinematic features, a typical
174 normal gait cycle was adjusted to these optimum features using the curve fitting technique and the optimized gait
175 pattern was reconstructed. Figure 3 shows schematic of the proposed combined TDNN-GA methodology in this study.

176 3. Results

177 3.1. Network training

178 A four-layer TDNN with four delay units at its input layer , 20 hidden neurons at the first hidden layer and 15
179 hidden neurons at the second one, was trained using 70% of the generated data base. Then, it was validated and tested
180 with the remaining 30%. Figure 4 shows the average performance of the proposed network over 100 training and testing
181 repetitions, each time with a random selection of subsets(Iyer and Rhinehart, 1999). According to the results, the TDNN
182 could accurately predict CPRESS-max values for the training, validation and test subsets. Pearson correlation
183 coefficients, between network predictions (Y axis) and real outputs (X axis), were all above $p=0.98$. Figures 4a, b show
184 that the network learned the nonlinear interaction of kinematics and contact pressure variables ($p=0.99$). Figure 4c
185 shows that the network could predict the CPRESS-max values corresponding to new sets of kinematics which were not
186 included in the training data space ($p=0.98$).

187 3.2. Optimization problem

188 The crossover fraction substantially affects the convergence of GA. Optimization was therefore run for a
189 variety of different values of crossover fraction ranged from 0 to 1 in the step size of 0.05. The crossover fraction of
190 0.85 led to the lowest CPRESS-max value (see Figure 5). Thus, this value was adopted for the rest of this study. In the
191 first optimization problem, knee flexion angle was bounded within *normal* walking. The algorithm was terminated after
192 75 populations due to stall generation criterion, in which the average change of the objective value (CPRESS-max)
193 was less than 10^{-6} (function tolerance) over 50 populations (stall generations). Figure 6a shows the mean and the best
194 CPRESS-max values associated with each population. After successful convergence of the algorithm, TDNN-GA
195 achieved the lowest CPRESS-max value of 25.58 MPa for the best individual of the last population.

196 Using the curve fitting technique, a representative normal gait cycle was updated due to the obtained optimum
197 kinematic features and the optimized gait pattern was reconstructed (Figure 7). The optimized kinematics laid within
198 the experimental gait patterns suggesting that it would be feasible for the subject to execute the optimized pattern.
199 Using multi-body dynamics analysis, the corresponding joint loadings were computed and compared with the span of
200 experimental values (Figure 8). Results show that lower extremity joints (ankle, knee and hip) underwent realistic
201 loading conditions i.e. within and with similar pattern to the *experimental* gait trials. Particularly, hip joint loading was
202 generally low in the anterior-posterior direction. A general reduction at the anterior-posterior component of knee joint
203 loading and significant reduction at its medial-lateral component around 40%-60% of the gait cycle occurred.
204 Moreover, the medial-lateral component of ankle joint loading was significantly decreased accompanied with a
205 reduction at its anterior-posterior component around 40%-60% of the gait cycle. Figure 9 shows the resultant
206 distribution of the maximum contact pressure over the medial tibiofemoral joint over the entire gait cycle. The
207 maximum contact pressure was reduced by 21.8% compared to the *normal* walking, while previously published gait
208 modifications were fairly ineffective to decrease the contact pressure magnitudes.

209 In the second optimization problem, X_L and X_U were modified and the knee joint flexion was bounded between
210 *normal* and *medial thrust* patterns. The GA achieved the convergence value of 24.61 MPa after 77 populations (Figure
211 6b). Reconstructed gait kinematics and the resultant joint loading patterns are presented in Figures 7 and 8 respectively.
212 Results demonstrate that the second optimized gait pattern also laid within the span of executable gait patterns. The
213 second optimized gait modification led to a significant reduction at the three dimensional hip joint loading (anterior-
214 posterior, proximal-distal and medial-lateral) around 0-25% of the gait cycle. This pattern also led to an overall
215 reduction at anterior-posterior component of the knee joint loading. Anterior-posterior and medial-lateral components
216 of the ankle joint loading were substantially low at 0-25% of the gait cycle, however ankle joint loading was slightly
217 increased around 40%-60% of the gait cycle. By comparison, the second optimization problem yielded to a more
218 effective gait modification pattern that better reduced the magnitude of the contact pressure by 25% (Figure 9).

219 4. Discussion

220 4.1. Hybrid neural network-genetic algorithm

221 Neural network was employed for a two-fold purpose: *first*, it modelled the highly nonlinear relationship
222 between gait kinematics and contact pressure; *second*, it served as a real-time cost function that allowed the
223 optimization algorithm to be performed in a reasonable computation time. A recent study by Lu et al. (2013)
224 demonstrated that the dynamic structure of a time delay neural network was preferred for modelling the relation

225 between tibiofemoral cartilage load (input) and von Mises stress (output), compared to the traditional static feed
226 forward neural network. Therefore, this structure was used in this study. Moreover, neural network has been used to
227 calculate joint loading from ground reaction forces and gait kinematics (Ardestani et al., 2013, Ardestani et al., 2014)
228 and ground reaction force from gait kinematics (Oh et al., 2013, Ren et al., 2008). In this study, neural network was
229 employed to calculate the contact pressure from gait kinematics. The high correlation that was found between the target
230 values and network predictions for validation and test subsets reassures the reliability of the proposed structure. The
231 TDNN in turn necessitated involving the GA as the optimization technique. In fact, other classical optimization
232 approaches mainly rely on iterative derivation of an explicit cost function however TDNN modelled the problem non-
233 explicitly.

234 **4. 2. Current research contribution**

235 There are a number of implications on the gait modification and optimization both in terms of methodology and
236 findings. Major limitations of the previous studies were addressed in the present research. *First*, compared to previous
237 studies in which iterative “trial-and-error” MBD analysis has been used, this study presented a cost-effective
238 computational alternative. TDNN provided a real-time cost function for the GA that could rapidly evaluate the contact
239 pressure associated with each potential gait pattern. Moreover, GA is a stochastic direct search method in which the
240 search data space is modified iteratively. This in turn reduced the computational effort required to find the optimized
241 solution. It should be pointed out that although various gait modifications have been developed in association with
242 knee joint offloading, none of them have yet been accepted as a general modification strategy. In fact, due to the large
243 inter-patient variability, reported in gait kinematics and joint loading patterns(Kutzner et al., 2010, Taylor et al., 2004)
244 , gait rehabilitation strategies should be determined patient specifically. Hence, to design a gait modification strategy,
245 it is crucial that the proposed computational method is cost-effective and easy to recreate.

246 Second, unlike the previous studies in which KAM reduction has been the principal goal of gait modification, here,
247 contact pressure was adopted as a more accurate criterion for knee joint offloading. This in turn built more confidence
248 in the efficiency of the proposed gait modification. Previous gait modifications were mainly designed to reduce knee
249 joint moment. Although these modification patterns could decrease knee joint loading, none of them could decrease
250 contact pressure at the knee joint bearing surfaces whilst the proposed gait pattern in this study could effectively
251 decrease the contact pressure by up to 25% (see Figure 9).

252 Third, whilst previous studies have debated on the influence of increasing knee flexion, this study could address
253 the contribution of knee flexion angle to the knee joint offloading in a systematic manner. Two optimizations were

254 performed: first, knee flexion angle was kept within normal patterns to investigate whether it was possible to
255 decrease knee joint loading through adjacent joints effects. Second, knee flexion was allowed for a non-significant
256 increase. Results showed that in the first optimized gait, contact pressure was reduced by up to 21% whilst knee flexion
257 was preserved within normal walking. In the second optimized pattern, a more effective pressure reduction (25%) was
258 achieved with a slight increase in the knee flexion (up to 8°) at the cost of considerable increase in the ankle joint
259 forces at 40-60% of the gait cycle. This observation is consistent with previous studies (Fregly et al., 2007) and suggests
260 that perhaps the first optimization pattern in which joint reaction forces were within the experimental range might be
261 more physiologically feasible. Allowing the knee flexion angle to be more increased ($>10^\circ$) led to higher ankle joint
262 loading and a gradual reduction in the contact area which in turn increased contact pressure.

263 Overall, hip adduction, ankle flexion, subtalar eversion, pelvis posterior rotation and pelvis medial-lateral rotation were
264 increased during the stance phase for both optimized gait patterns (see Figure 7). However it should be noted that the
265 exact amount of kinematic changes, compared to normal gait, was not reported in this study since specific gait
266 rehabilitation, designed for a particular subject, may not be equally applicable for other patients. Therefore, the
267 quantitative amount of kinematic variations, compared to normal gait, was not focused in this study.

268 4. 3. Limitations

269 There were several limitations in this study: (1) there was a lack of clinical investigation on the estimated
270 kinematics. Nevertheless, from a technical point of view, the predicted kinematic waveforms are expected to be feasible
271 since the TDNN was trained based on executable walking patterns. Once the network learns this dynamics, it uses this
272 dynamics as the acting function to respond to new sets of inputs. Therefore, it is unlikely that it would generate highly
273 aberrant kinematics. Regardless, further investigations are required to test whether the predicted kinematics is feasible
274 to implement for compensatory or unexpected effects on the other joints or the contra-lateral limb; (2) rigid body
275 constraints were applied to both the femoral and tibia components. Halloran et al.(2005) showed that rigid body analysis
276 of the tibiofemoral knee implant can calculate contact pressure in an acceptable consistence with a full deformable
277 model whilst rigid body analysis would be much more time-efficient. Therefore, in order to produce the training data
278 base, required to train the neural network, rigid body constraints were applied. This was consistent with the present
279 multi-body dynamics analysis in which no detailed modelling on the knee implant was included; (3) a typical knee
280 implant was adopted in the present study. Although this implant has been widely used in literature (Clayton et al., 2006,
281 Dalury et al., 2008, Ranawat et al., 2004, Willing and Kim, 2011) , its dimensions were different from the original knee
282 prosthesis by which the subject was implanted. In fact, the subject was implanted with a custom-made sensor-based
283 prosthesis which was specifically produced to measure *in vivo* knee joint loading(Fregly et al., 2012). Accordingly, in

284 this study , a typical commercial knee implant was preferred to test the efficiency of proposed knee rehabilitation
285 patterns. Nevertheless, the proposed methodology should be equally applicable to other implant geometries and (4) the
286 knee joint was modelled with only one DOF (flexion-extension). Although six DOFs are possible for the knee joint,
287 the dominant movement of the knee joint takes place in the sagittal plane and knee joint has been widely simplified as
288 a hinge joint, especially for the knee rehabilitation design purposes (Ackermann and van den Bogert, 2010, Anderson
289 and Pandy, 2001, Fregly et al., 2007).

290 **5. Conclusion**

291 A time-delay neural network was embedded in a genetic algorithm to predict a gait pattern that would minimize
292 the contact pressure at the knee joint bearing surfaces. The proposed algorithm suggested an optimum gait pattern in
293 which hip adduction, ankle flexion, subtalar eversion, pelvis posterior rotation and pelvis medial-lateral rotation were
294 slightly increased during the stance phase. Compared to the available gait rehabilitations, the proposed gait pattern
295 could decrease the knee contact pressure by up to 25%. Compared to the conventional MBD-based framework in gait
296 rehabilitation design, the present methodology facilitated a more practical and reliable design procedure at a lower
297 computational cost :(1) instead of using knee adduction moment, contact pressure was considered as a more accurate
298 criterion which led to a more efficient gait modification, (2) using the time-delay neural network, the proposed
299 computational framework was considerably faster and time-efficient. The computational framework therefore can be
300 easily repeated for any given subject. Moreover, (3) the conflicting effect of the knee flexion was addressed through
301 two systematic optimization frameworks: (i) knee joint may be offloaded without any changes in the knee flexion angle
302 (ii) a slight increase in the knee flexion angle (up to 8°) might better reduce contact pressure but at the cost of ankle
303 joint over loading and (iii) more increase in the knee flexion angle (more than 10°) reduced the contact area and
304 yielded to an increment in the contact pressure.

305 Various future direction from this study can be considered: (1) on the methodological level, more rigorous
306 tribological metrics (e.g. wear), constraints (e.g. energy expenditure) or gait balance requirements can be included into
307 the computational framework to enhance the predications; (2) on the validation level, further clinical studies are
308 required to validate the finding of such studies; (3) on a wider application level, the proposed methodology in this study
309 has wider implications in design and development of rehabilitation protocols for broader numbers of subjects and other
310 joints such as hip and ankle.

311 **Conflict of interest statement**

312 The authors have no conflict of interests to be declared.

313 **Acknowledgments**

314 This work was supported by “the Fundamental Research Funds for the Central Universities and national
 315 Natural Science Foundation of China [E050702, 51323007]”.The authors gratefully acknowledge " Grand Challenge
 316 Competition to Predict In Vivo Knee Loads" for releasing the experimental data. The authors would like to thank
 317 Shanghai Gaitech Scientific Instruments Co. Ltd for supplementing AnyBody software used in this study.

318 **References**

- 319 ABDELGAIED, A., LIU, F., BROCKETT, C., JENNINGS, L., FISHER, J. & JIN, Z. 2011. Computational
 320 wear prediction of artificial knee joints based on a new wear law and formulation. *Journal of*
 321 *biomechanics*, 44, 1108-1116.
- 322 ACKERMANN, M. & VAN DEN BOGERT, A. J. 2010. Optimality principles for model-based prediction of
 323 human gait. *Journal of biomechanics*, 43, 1055-1060.
- 324 ANDERSON, F. C. & PANDY, M. G. 2001. Dynamic optimization of human walking. *TRANSACTIONS-*
 325 *AMERICAN SOCIETY OF MECHANICAL ENGINEERS JOURNAL OF BIOMECHANICAL*
 326 *ENGINEERING*, 123, 381-390.
- 327 ARDESTANI, M. M., CHEN, Z., WANG, L., LIAN, Q., LIU, Y., HE, J., LI, D. & JIN, Z. 2014. Feed forward
 328 artificial neural network to predict contact force at medial knee joint: Application to gait modification.
 329 *Neurocomputing*, 139, 114-129.
- 330 ARDESTANI, M. M., ZHANG, X., WANG, L., LIAN, Q., LIU, Y., HE, J., LI, D. & JIN, Z. 2013. Human
 331 lower extremity joint moment prediction: A wavelet neural network approach. *Expert Systems with*
 332 *Applications*.
- 333 ARMAND, S., WATELAIN, E., MERCIER, M., LENSEL, G. & LEPOUTRE, F.-X. 2006. Identification and
 334 classification of toe-walkers based on ankle kinematics, using a data-mining method. *Gait & posture*,
 335 23, 240-248.
- 336 BARRIOS, J. A., CROSSLEY, K. M. & DAVIS, I. S. 2010. Gait retraining to reduce the knee adduction
 337 moment through real-time visual feedback of dynamic knee alignment. *Journal of biomechanics*, 43,
 338 2208-2213.
- 339 BARRIOS, J. A. & DAVIS, I. S. A gait modification to reduce the external adduction moment at the knee: a
 340 case study. 31st Annual Meeting of the American Society of Biomechanics, Stanford, CA, paper,
 341 2007.
- 342 CAMPOLI, G., WEINANS, H. & ZADPOOR, A. A. 2012. Computational load estimation of the femur.
 343 *Journal of the Mechanical Behavior of Biomedical Materials*, 10, 108-119.
- 344 CLAYTON, R. A., AMIN, A. K., GASTON, M. S. & BRENKEL, I. J. 2006. Five-year results of the Sigma
 345 total knee arthroplasty. *The Knee*, 13, 359-364.

346 COLLINS, T. D., GHOUSSAYNI, S. N., EWINS, D. J. & KENT, J. A. 2009. A six degrees-of-freedom
347 marker set for gait analysis: repeatability and comparison with a modified Helen Hayes set. *Gait &*
348 *posture*, 30, 173-180.

349 CREABY, M. W., HUNT, M. A., HINMAN, R. S. & BENNELL, K. L. 2013. Sagittal plane joint loading is
350 related to knee flexion in osteoarthritic gait. *Clinical Biomechanics*, 28, 916-920.

351 D'LIMA, D. D., STEKLOV, N., FREGLY, B. J., BANKS, S. A. & COLWELL, C. W. 2008. In vivo contact
352 stresses during activities of daily living after knee arthroplasty. *Journal of Orthopaedic Research*, 26,
353 1549-1555.

354 DALURY, D. F., GONZALES, R. A., ADAMS, M. J., GRUEN, T. A. & TRIER, K. 2008. Midterm results
355 with the PFC Sigma total knee arthroplasty system. *The Journal of Arthroplasty*, 23, 175-181.

356 FRANSEN, M. Rehabilitation after knee replacement surgery for osteoarthritis. *Seminars in Arthritis and*
357 *Rheumatism*, 2011. Elsevier, 93.

358 FREGLY, B. J., BESIÉ, T. F., LLOYD, D. G., DELP, S. L., BANKS, S. A., PANDY, M. G. & D'LIMA, D.
359 D. 2012. Grand challenge competition to predict in vivo knee loads. *Journal of Orthopaedic Research*,
360 30, 503-513.

361 FREGLY, B. J., D'LIMA, D. D. & COLWELL, C. W. 2009. Effective gait patterns for offloading the medial
362 compartment of the knee. *Journal of Orthopaedic Research*, 27, 1016-1021.

363 FREGLY, B. J., REINBOLT, J. A., ROONEY, K. L., MITCHELL, K. H. & CHMIELEWSKI, T. L. 2007.
364 Design of patient-specific gait modifications for knee osteoarthritis rehabilitation. *Biomedical*
365 *Engineering, IEEE Transactions on*, 54, 1687-1695.

366 GATES, D. H., DINGWELL, J. B., SCOTT, S. J., SINITSKI, E. H. & WILKEN, J. M. 2012a. Gait
367 characteristics of individuals with transtibial amputations walking on a destabilizing rock surface.
368 *Gait & posture*, 36, 33-39.

369 GATES, D. H., WILKEN, J. M., SCOTT, S. J., SINITSKI, E. H. & DINGWELL, J. B. 2012b. Kinematic
370 strategies for walking across a destabilizing rock surface. *Gait & Posture*, 35, 36-42.

371 GOLDBERG, D. 1989. *Genetic Algorithms in Search, Optimization, and Machine Learning*, Addison-Wesley,
372 Reading, MA, 1989.

373 HALLORAN, J. P., ACKERMANN, M., ERDEMIR, A. & VAN DEN BOGERT, A. J. 2010. Concurrent
374 musculoskeletal dynamics and finite element analysis predicts altered gait patterns to reduce foot
375 tissue loading. *Journal of biomechanics*, 43, 2810-2815.

376 HALLORAN, J. P., PETRELLA, A. J. & RULLKOETTER, P. J. 2005. Explicit finite element modeling of
377 total knee replacement mechanics. *Journal of biomechanics*, 38, 323-331.

378 HAMBLI, R. 2010. Application of neural networks and finite element computation for multiscale simulation
379 of bone remodeling. *Journal of biomechanical engineering*, 132, 114502.

380 HAMBLI, R. 2011. Numerical procedure for multiscale bone adaptation prediction based on neural networks
381 and finite element simulation. *Finite elements in analysis and design*, 47, 835-842.

382 HUNT, M., BIRMINGHAM, T., BRYANT, D., JONES, I., GIFFIN, J., JENKYN, T. & VANDERVOORT, A.
383 2008. Lateral trunk lean explains variation in dynamic knee joint load in patients with medial
384 compartment knee osteoarthritis. *Osteoarthritis and Cartilage*, 16, 591-599.

385 ISAAC, D., FALODE, T., LIU, P., I'ANSON, H., DILLOW, K. & GILL, P. 2005. Accelerated rehabilitation
386 after total knee replacement. *The knee*, 12, 346-350.

387 IYER, M. S. & RHINEHART, R. R. 1999. A method to determine the required number of neural-network
388 training repetitions. *Neural Networks, IEEE Transactions on*, 10, 427-432.

389 KLEIN, G. R., LEVINE, H. B. & HARTZBAND, M. A. Pain Management and Accelerated Rehabilitation
390 After Total Knee Arthroplasty. *Seminars in Arthroplasty*, 2008. Elsevier, 248-251.

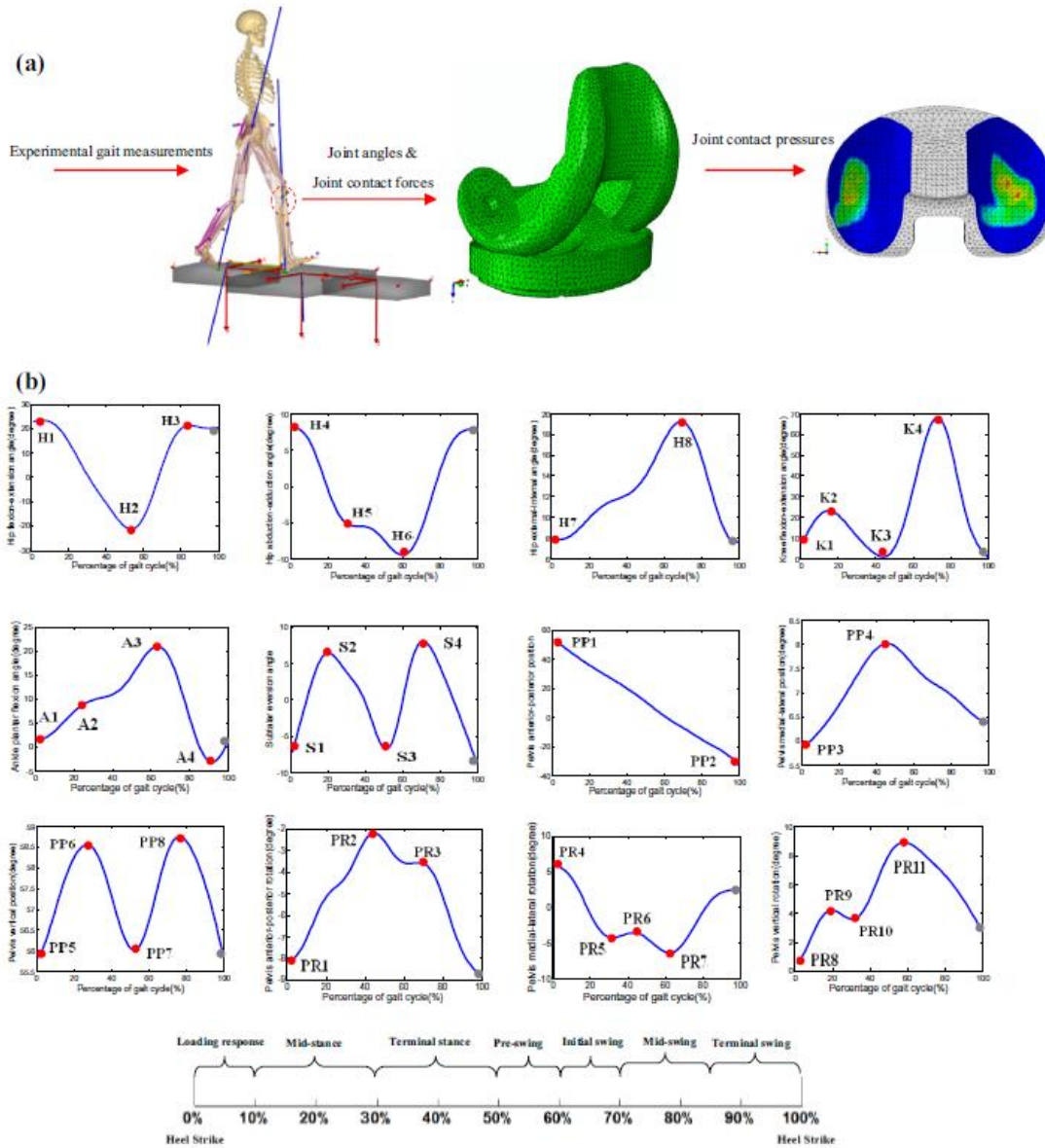
391 KLEIN HORSMAN, M. D. 2007. *The Twente lower extremity model: consistent dynamic simulation of the*
392 *human locomotor apparatus*, University of Twente.

- 393 KUTZNER, I., HEINLEIN, B., GRAICHEN, F., BENDER, A., ROHLMANN, A., HALDER, A., BEIER,
394 A. & BERGMANN, G. 2010. Loading of the knee joint during activities of daily living measured
395 in vivo in five subjects. *Journal of biomechanics*, 43, 2164-2173.
- 396 LIN, C.-J., LAI, K.-A., CHOU, Y.-L. & HO, C.-S. 2001. The effect of changing the foot progression angle
397 on the knee adduction moment in normal teenagers. *Gait & Posture*, 14, 85-91.
- 398 LU, Y., PULASANI, P. R., DERAKHSHANI, R. & GUESS, T. M. 2013. Application of neural networks for
399 the prediction of cartilage stress in a musculoskeletal system. *Biomedical Signal Processing and*
400 *Control*, 8, 475-482.
- 401 MILLER, M. F. 1993. A scaled conjugate gradient algorithm for fast supervised learning. *Neural networks*,
402 6, 525-533.
- 403 M NDERMANN, A., ASAY, J. L., M NDERMANN, L. & ANDRIACCHI, T. P. 2008. Implications of
404 increased medio-lateral trunk sway for ambulatory mechanics. *Journal of biomechanics*, 41, 165-170.
- 405 MOFFET, H., COLLET, J.-P., SHAPIRO, S. H., PARADIS, G., MARQUIS, F. & ROY, L. 2004.
406 Effectiveness of intensive rehabilitation on functional ability and quality of life after first total knee
407 arthroplasty: a single-blind randomized controlled trial. *Archives of physical medicine and*
408 *rehabilitation*, 85, 546-556.
- 409 MONT, M. A., BONUTTI, P. M., SEYLER, T. M., PLATE, J. F., DELANOIS, R. E. & KESTER, M. The
410 future of high performance total hip arthroplasty. *Seminars in Arthroplasty*, 2006. Elsevier, 88-92.
- 411 NAITO, K. & TORII, S. 2005. Effects of laterally wedged insoles on knee and subtalar joint moments. *Arch*
412 *Phys Med Rehabil*, 86.
- 413 OH, S. E., CHOI, A. & MUN, J. H. 2013. Prediction of ground reaction forces during gait based on kinematics
414 and a neural network model. *Journal of biomechanics*, 46, 2372-2380.
- 415 RAHMANN, A. E., BRAUER, S. G. & NITZ, J. C. 2009. A specific inpatient aquatic physiotherapy program
416 improves strength after total hip or knee replacement surgery: a randomized controlled trial. *Archives*
417 *of physical medicine and rehabilitation*, 90, 745-755.
- 418 RANAWAT, A. S., ROSSI, R., LORETI, I., RASQUINHA, V. J., RODRIGUEZ, J. A. & RANAWAT, C. S.
419 2004. Comparison of the PFC Sigma fixed-bearing and rotating-platform total knee arthroplasty in
420 the same patient: short-term results. *The Journal of arthroplasty*, 19, 35-39.
- 421 REN, L., JONES, R. K. & HOWARD, D. 2008. Whole body inverse dynamics over a complete gait cycle
422 based only on measured kinematics. *Journal of Biomechanics*, 41, 2750-2759.
- 423 SCHIPPLEIN, O. & ANDRIACCHI, T. 1991. Interaction between active and passive knee stabilizers during
424 level walking. *Journal of Orthopaedic Research*, 9, 113-119.
- 425 SHULL, P. B., SHULTZ, R., SILDER, A., DRAGOO, J. L., BESIER, T. F., CUTKOSKY, M. R. & DELP, S.
426 L. 2012. Toe-in gait reduces the first peak knee adduction moment in patients with medial
427 compartment knee osteoarthritis. *Journal of biomechanics*.
- 428 SIMIC, M., HINMAN, R. S., WRIGLEY, T. V., BENNELL, K. L. & HUNT, M. A. 2011. Gait modification
429 strategies for altering medial knee joint load: A systematic review. *Arthritis Care & Research*, 63,
430 405-426.
- 431 SIMONSEN, E. B., MOESBY, L. M., HANSEN, L. D., COMINS, J. & ALKJAER, T. 2010. Redistribution
432 of joint moments during walking in patients with drop-foot. *Clinical Biomechanics*, 25, 949-952.
- 433 TAYLOR, W. R., HELLER, M. O., BERGMANN, G. & DUDA, G. N. 2004. Tibio - femoral loading during
434 human gait and stair climbing. *Journal of Orthopaedic Research*, 22, 625-632.
- 435 VAN DEN NOORT, J. C., SCHAFFERS, I., SNIJDERS, J. & HARLAAR, J. 2013. The effectiveness of
436 voluntary modifications of gait pattern to reduce the knee adduction moment. *Human movement*
437 *science*.
- 438 VAUGHAN, C. L., DAVIS, B. L. & O'CONNOR, J. C. 1992. *Dynamics of human gait*, Human Kinetics
439 Publishers USA.

- 440 WALTER, J. P., D'LIMA, D. D., COLWELL, C. W. & FREGLY, B. J. 2010. Decreased knee adduction
441 moment does not guarantee decreased medial contact force during gait. *Journal of Orthopaedic*
442 *Research*, 28, 1348-1354.
- 443 WANG, T.-M., YEN, H.-C., LU, T.-W., CHEN, H.-L., CHANG, C.-F., LIU, Y.-H. & TSAI, W.-C. 2009.
444 Bilateral knee osteoarthritis does not affect inter-joint coordination in older adults with gait deviations
445 during obstacle-crossing. *Journal of biomechanics*, 42, 2349-2356.
- 446 WILLING, R. & KIM, I. Y. 2011. Design optimization of a total knee replacement for improved constraint
447 and flexion kinematics. *Journal of Biomechanics*, 44, 1014-1020.
- 448 WILLSON, J., TORRY, M. R., DECKER, M. J., KERNOZEK, T. & STEADMAN, J. 2001. Effects of
449 walking poles on lower extremity gait mechanics. *Medicine and science in sports and exercise*, 33,
450 142-147.
- 451 ZADPOOR, A. A., CAMPOLI, G. & WEINANS, H. 2012. Neural network prediction of load from the
452 morphology of trabecular bone. *Applied Mathematical Modelling*.
- 453 ZENI JR, J., MCCLELLAND, J. & SNYDER-MACKLER, L. 2011. 193 A NOVEL REHABILITATION
454 PARADIGM TO IMPROVE MOVEMENT SYMMETRY AND MAXIMIZE LONG-TERM
455 OUTCOMES AFTER TOTAL KNEE ARTHROPLASTY. *Osteoarthritis and Cartilage*, 19, S96-S97.
- 456

457

458 Fig. 1. (a) Experimental gait measurements were imported into multi-body dynamics analysis to calculate
459 joint kinematics/kinetics which were then used by finite element analysis to calculate contact pressure (b)
460 joint angles were parameterized by extremum features (red circles). Due to the periodicity of the gait, joint
461 angle values at the end of the gait cycle (gray points) were equal to the initial values at 0% of the gait cycle
462 except for pelvis position. (For interpretation anterior–posterior of the references to color in this figure



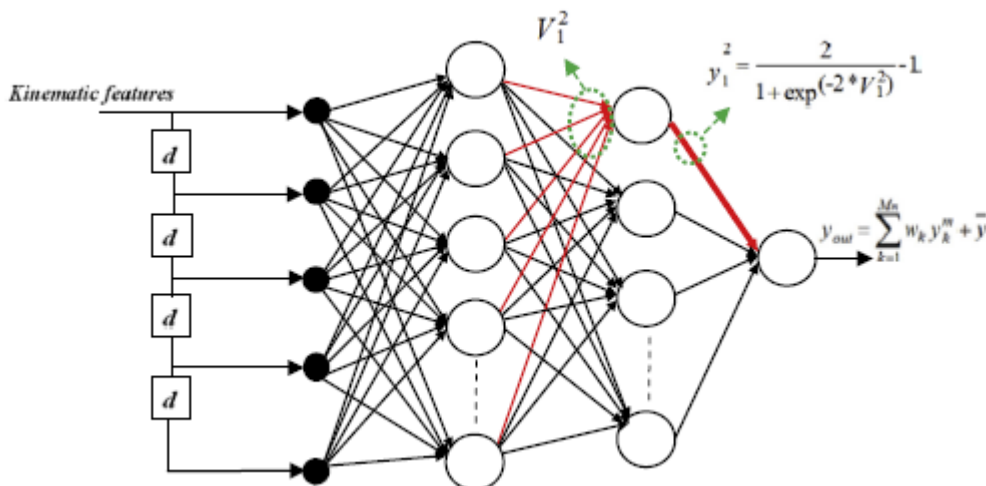
464

465

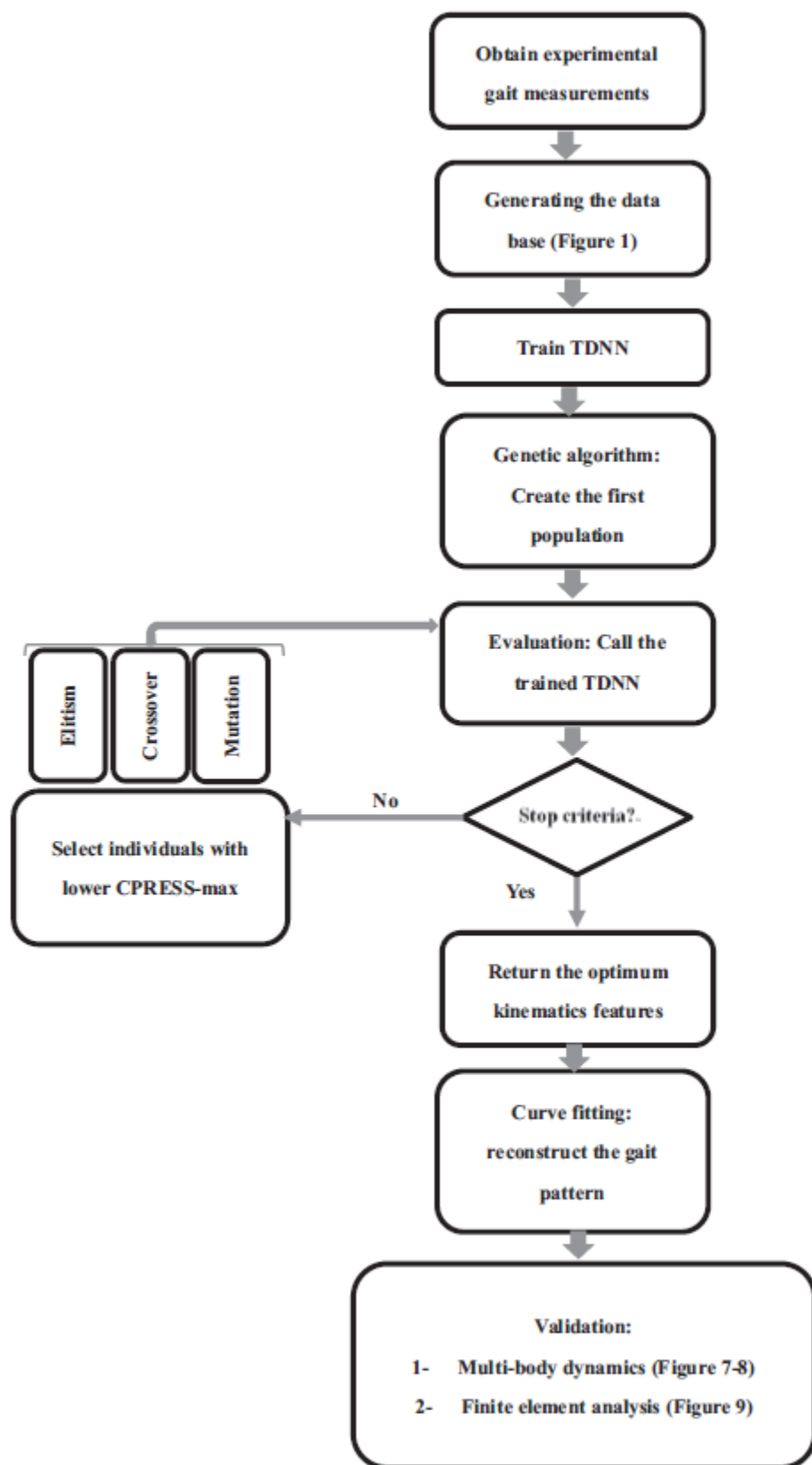
466

467

Fig. 2. A schematic diagram of a four-layer TDNN used in this study. The network calculated the maximum values of contact pressure (output) based on gait features (inputs).



468



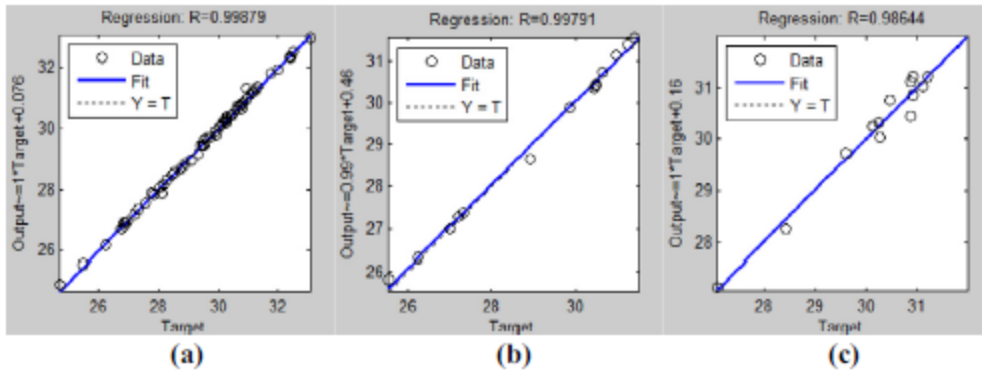
470

471

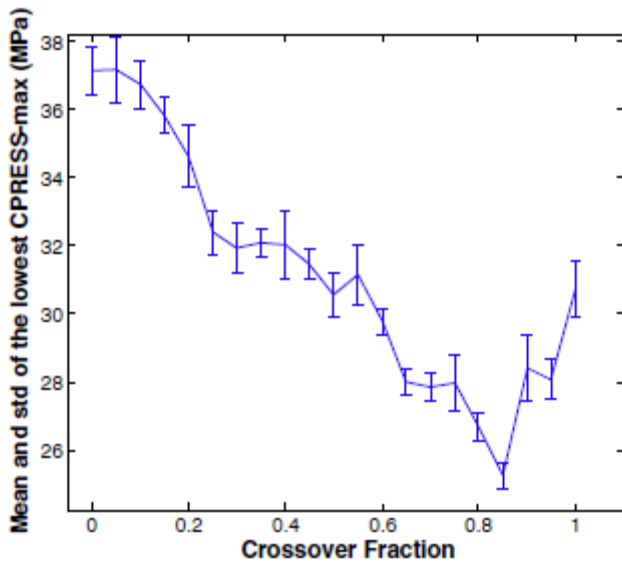
472

473

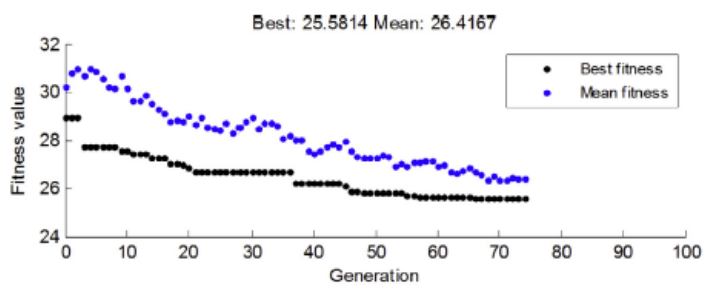
474 Fig. 4. Network predictions vs. actual CPRESS-max values for (a) train (b) validation and (c) test subsets.



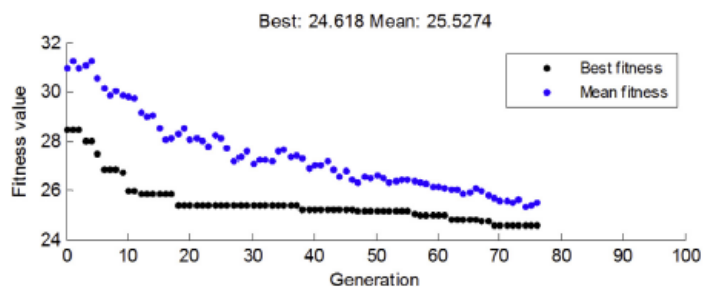
477 Fig. 5. Mean and standard deviation of the optimized CPRESS-max for different values of crossover
 478 fraction in the GA process.



495 Fig. 6. Convergence of the GA for (a) the first optimization problem in which the knee flexion angle was
496 bounded to normal patterns, (b) the second optimization problem in which the knee flexion angle was
497 allowed to increase beyond normal pattern. "Fitness" refers to the calculated value of CPRESS-max for
498 each individual.



(a)



(b)

499

500

501

502

503

504

505

506

507

508

509

510

511

512

513

514

515

516

517

518

519

520

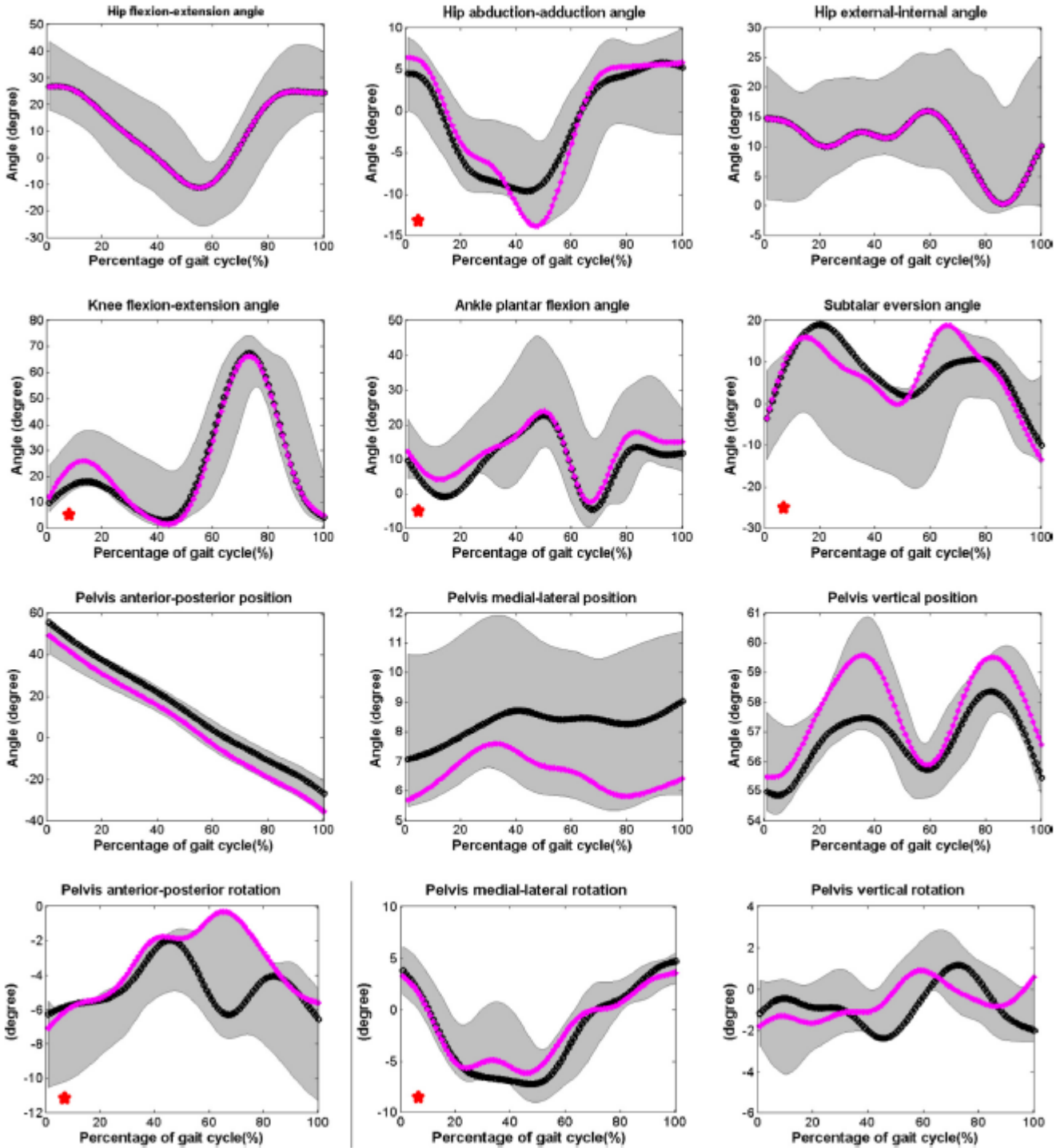
521

522

523

524

526 Fig. 7. Kinematics of the first optimized gait pattern (black line) and the second optimized pattern (pink line) laid within the extent of experimental gait trials (gray span). Those kinematics that underwent
527 considerable changes have been marked by . (For interpretation of the references to color in this figure
528 legend, the reader is referred to the web version of this article.)
529



530

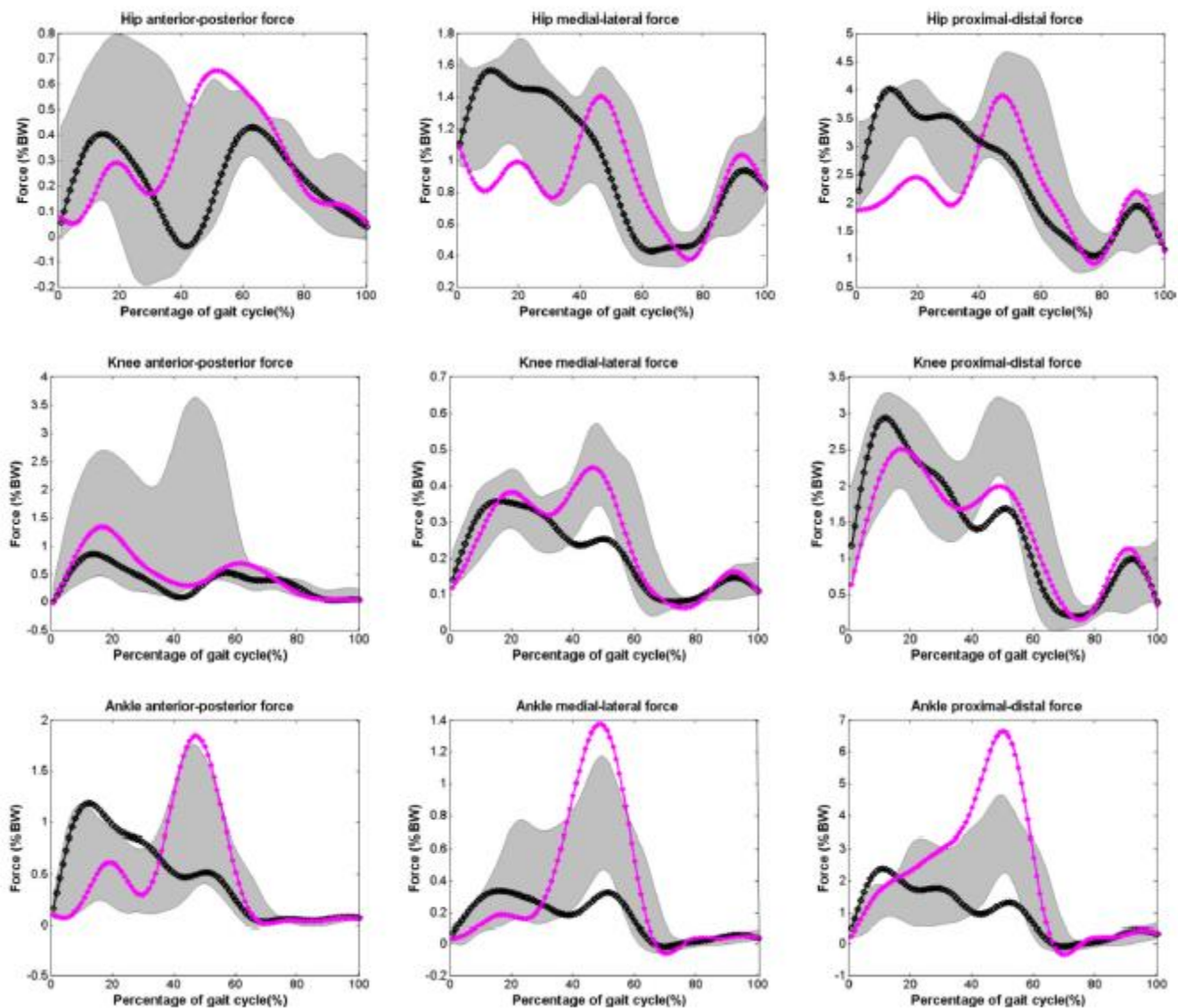
531

532

533

534

535 Fig. 8. Resultant joint contact forces of the first optimized gait pattern (black line) and the second
536 optimized pattern (pink line) laid within the extent of experimental gait trials (gray span). (For interpretation
537 of the references to color in this figure legend, the reader is referred to the web version of this article.)



538

539

540

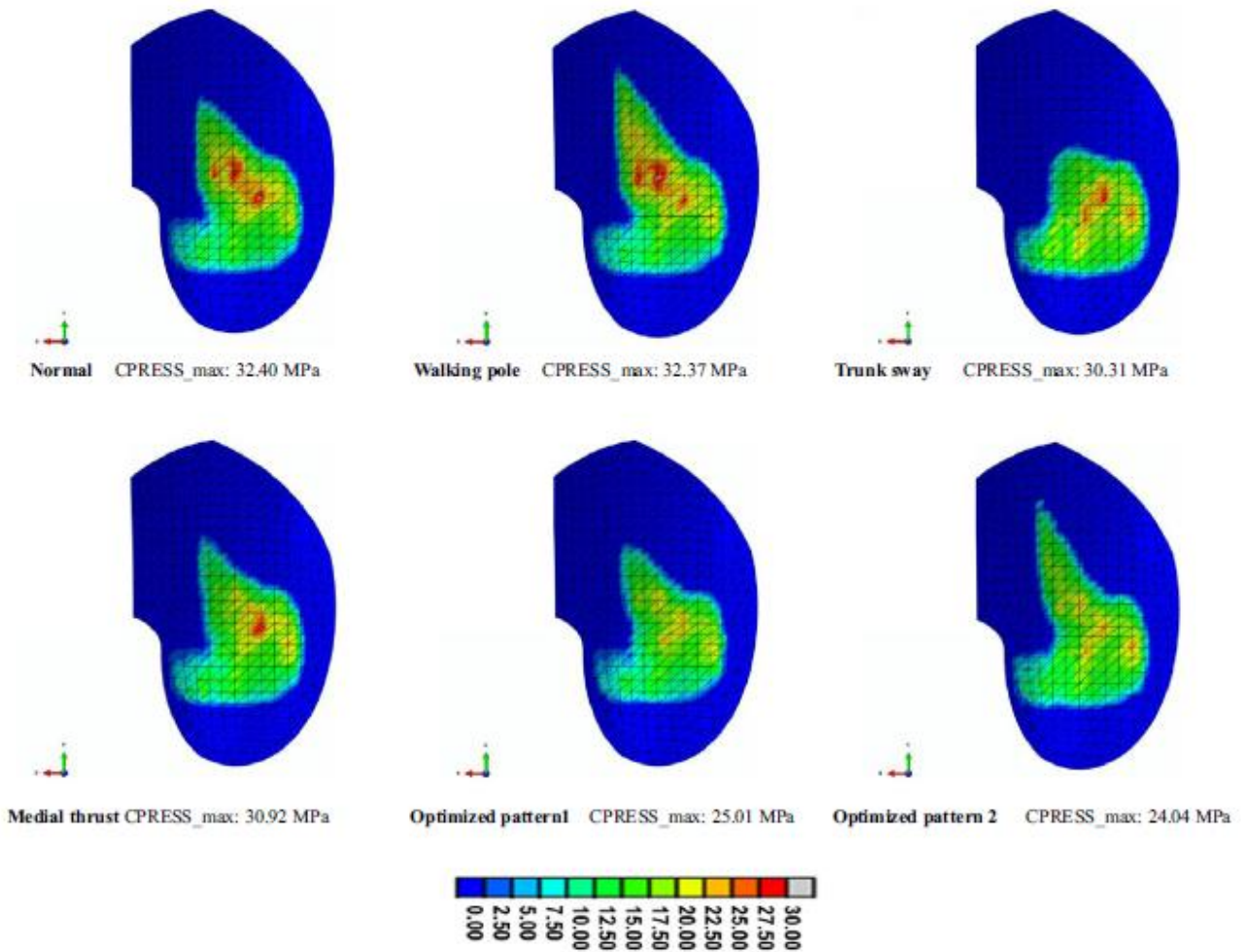
541

542

543

544

547 Fig. 9. The resultant maximum values of contact pressures for the optimized gait patterns vs. contact
548 pressures obtained from normal gait and other previously published gait modifications.



563
564
565
566
567
568
569
570

Table 1 Description of gait kinematic features.

Table 1
Description of gait kinematic features.

Joint	Kinematic feature	Description
Hip	H1	Hip flexion at initial contact
Hip	H2	Maximum hip extension at stance
Hip	H3	Maximum hip flexion at swing phase
Hip	H4	Hip abduction at initial contact
Hip	H5	Maximum hip adduction at midstance phase
Hip	H6	Maximum hip adduction at stance phase
Hip	H7	Hip external rotation at initial contact
Hip	H8	Maximum hip internal rotation at swing phase
Knee	K1	Knee flexion at initial contact
Knee	K2	Maximum knee flexion at stance
Knee	K3	Maximum knee extension at stance
Knee	K4	Maximum knee flexion at swing phase
Ankle	A1	Ankle flexion at initial contact
Ankle	A2	Maximum ankle dorsiflexion at midstance
Ankle	A3	Maximum ankle dorsiflexion at stance
Ankle	A4	Maximum ankle plantar flexion at swing phase
Subtalar	S1	Subtalar inversion at initial contact
Subtalar	S2	Maximum subtalar eversion at stance
Subtalar	S3	Maximum subtalar inversion at stance
Subtalar	S4	Maximum subtalar eversion at swing
Pelvis	PP1	Maximum posterior tilt of pelvis
Pelvis	PP2	Maximum anterior tilt of the pelvis
Pelvis	PP3	Maximum lateral obliquity of the pelvis
Pelvis	PP4	Maximum medial obliquity of the pelvis
Pelvis	PP5	Pelvis vertical position at initial contact
Pelvis	PP6	Maximum pelvis upward position at stance
Pelvis	PP7	Maximum pelvis downward position at stance
Pelvis	PP8	Maximum pelvis upward position at swing
Pelvis	PR1	Pelvis anterior rotation at initial contact
Pelvis	PR2	Maximum pelvis posterior rotation at stance
Pelvis	PR3	Maximum pelvis posterior rotation at swing
Pelvis	PR4	Pelvis medial rotation at initial contact
Pelvis	PR5	Maximum pelvis lateral rotation at stance
Pelvis	PR6	Maximum pelvis medial rotation at stance
Pelvis	PR7	Maximum pelvis lateral rotation at swing
Pelvis	PR8	Pelvis axial rotation at initial contact
Pelvis	PR9	Maximum pelvis axial rotation to the left at stance
Pelvis	PR10	Minimum pelvis axial rotation to the right at stance
Pelvis	PR11	Maximum pelvis axial rotation to the left at swing

571

572 Table 2 Genetic algorithm settings in MATLAB.

Table 2
Genetic algorithm settings in MATLAB.

Genetic algorithm parameter	Value
Population size	50
Scaling function	Rank
Selection function	Tournament
Elite count	2
Crossover fraction	0.85
Crossover function	Single point
Mutation function	Adaptive feasible
Maximum number of generations	100

573